THE JOURNAL OF PHYSICAL CHEMISTRY B

Article

pubs.acs.org/JPCB

A Simple AIMD Approach to Derive Atomic Charges for Condensed Phase Simulation of Ionic Liquids

Yong Zhang and Edward J. Maginn*

Department of Chemical and Biomolecular Engineering, University of Notre Dame, Notre Dame, Indiana, 46556, United States

ABSTRACT: The atomic charges for two ionic liquids (ILs), 1-*n*-butyl-3-methylimidazolium hexafluorophosphate ([BMIM][PF6]) and 1-ethyl-3-methylimidazolium hexafluorophosphate ([EMIM][PF6]), were derived from periodic crystal phase calculations with density functional theory (DFT) and plane wave basis sets (denoted as "AIMD-c charge"). For both ILs, the total charge was found to be ±0.8 e for the cation and anion, respectively, due to the charge transfer between ions and polarization caused by the environment. These atomic charges were used in a force field developed within the general Amber force field framework. Using this force field, static, dynamic, and thermodynamic properties were computed for the two ILs using molecular dynamics simulation. The results were compared against results obtained using the same Amber force field but four different sets of partial charges, denoted as full charge, scaled charge, AIMD-l charge, and AIMD-b charge, respectively. The full charge was derived from quantum chemistry calculation of isolated ions in a vacuum and resulted in a total charge of unity on each ion. The scaled charge was obtained by uniformly scaling the full charge by 0.8. AIMD-l and AIMD-b charges were derived from liquid phase ab initio molecular dynamics simulations. The scaled charges have the same total charge on the ions as the AIMD-c charge but different distributions. It was found that simulation results not only depend on the total charge of each ion, but they are also sensitive to the charge distribution within an ion, especially for dynamic and thermodynamic properties. Overall, for the two ILs under study, the AIMD-c charge was found to predict experimental results better than the other four sets of charges, indicating that fitting charges from crystal phase DFT calculations, instead of extensive sampling of the liquid phase configurations, is a simple and reliable way to derive atomic charges for condensed phase ionic liquid simulations.

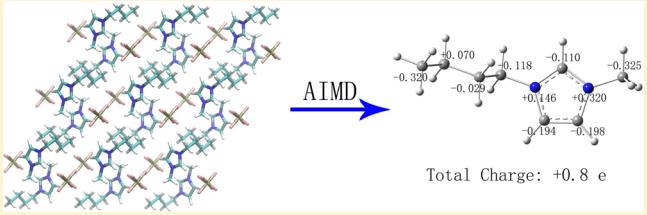

1. INTRODUCTION

Ionic liquids are salts that stay as liquid around room temperature. Due to their unique properties such as low melting points, negligible vapor pressure, nonflammability, and good ionic conductivity, the promising potential of ionic liquids for applications in various areas such as catalysis, separations, and electrochemistry has stimulated extensive study on this group of compounds during the past decade.[1−16]

Molecular simulation has been a powerful tool to provide an atomic-level understanding of complex systems. Ionic liquids have been widely studied using molecular simulation methods under various theoretical levels, ranging from static ab initio calculation,[17−19] ab initio molecular dynamics (AIMD),[14,20−30] polarizable molecular dynamics simulations,[7,9−11,31,32] to classical force field based simulations.[2,3,33−37]

Ab initio and density functional theory (DFT) provides accurate intra- and intermolecular interaction information of ionic liquids. However, due to their computationally demanding nature, application of these methods is usually limited to small systems and short time scales. On the other hand, molecular dynamics simulations based on a classical force field have been carried out on systems containing hundreds or thousands of IL pairs over nanosecond or even microsecond time scales. The reliability of such simulations highly depends on the force fields, which are usually developed using quantum calculations, experimental data, or both.

During the past decade, classical force fields have been developed for many ionic liquids.[38−48] Most of these force fields are based on existing parameters from OPLS,[49] Amber,[50] GROMOS,[51] or CHARMM.[52] For example, Canongia Lopes and co-workers have developed force fields for imidazolium based ILs based on OPLS-AA and Amber, and later extended their work to other ILs.[53−57] Force fields for imidazolium based ILs were also developed from Amber by Wang and co-workers.[42] United atom models have also been proposed.[58−61] Recently, Sambasivarao and Acevedo derived OPLS-AA compatible force fields for 68 ionic liquids.[62] Coarse grained models were also suggested for ionic liquids.[63,64]

It is believed that the unique properties of ionic liquids, such as low vapor pressure and good ionic conductivity, are rooted in their ionic nature, so the electrostatic interaction in ionic liquids has been given extra attention. Due to the charge transfer and polarizability of ionic species, the effective charges on cations and anions in bulk phases are smaller than unity.[11,38,65] This phenomenon was confirmed recently by experimental observations.[66,67] In ab initio or DFT calculations, the charge transfer or polarization is handled implicitly. In classical simulations, however, because the atomic charges are

Received: April 19, 2012
Revised: July 30, 2012
Published: August 2, 2012

usually derived from isolated ion quantum calculations carried out in a vacuum, the cation and anion usually have charges of +1 e and −1 e. Due to the strong electrostatic interaction, the simulated dynamic properties using unit charges were found to be slow compared to experimental measurements, unless other parameters were adjusted.[47]

Polarizable force fields have been developed to handle the effect of electronic polarizability in ILs. The first such force field was developed by Voth and co-workers for 1-ethyl-3-methylimidazolium nitrate ([EMIM][NO_3]).[7] Recently, polarizable force fields were developed for more ionic liquids by Borodin.[31] Using these force fields, the agreement of simulational results with experimental results is significantly improved. However, polarizable force fields are more complicated to develop and computationally more expensive than fixed charge models.

An alternative approximate treatment of charge transfer and polarizability within a classical force field framework is to use reduced static atomic charges. The first such attempt was carried out by Morrow and Maginn in their study on 1-*n*-butyl-3-methylimidazolium hexafluorophosphate ([BMIM][PF6]).[38] On the basis of the quantum calculation of an ion pair in a vacuum, a total charge of ±0.904 e was determined for the cation and anion. The computed quantities using such reduced charge parameters were found to be in good agreement with experimental results. Since then, force fields with reduced charges were proposed and applied in several simulations. Except for a few,[38,68] most of these force fields were obtained by applying a uniform scaling factor to the unit charges. The scaling factor was determined from liquid phase AIMD simulations,[65] fit to experimental density or other system properties,[69,70] or empirically chosen.[71−74] The atomic charge distributions within each molecule were left unchanged from those derived from quantum vacuum phase calculations.

As the charge transfer and polarization is caused by the environment in the bulk phase, Delle Site and co-workers have proposed a procedure to derive the atomic charges from liquid phase AIMD simulations directly.[75−77] The charges were derived using the Blöchl method for snapshots from a CPMD trajectory so that the liquid phase charge distribution is automatically involved. Clearly, the accuracy of this procedure depends on the proper sampling of the configurational space.

In spite of these efforts, force field development for ionic liquids, especially the atomic charges, is still a subject under development. In the current work, we present our effort toward the simple and reliable development of atomic charges for ionic liquids. The atomic charges of [BMIM][PF6] and [EMIM][PF6] (see Figure 1) were derived from AIMD simulations on their crystal phase (AIMD-c charge). The charges derived this way were compared with those derived from a vacuum phase quantum calculation which has the charge of unity ("full charge"), as well as those derived from liquid phase AIMD simulations (AIMD-l and AIMD-b charges, respectively). A set of reduced charges, obtained by uniformly scaling the full charge by 0.8 ("scaled charge"), was also included in the calculation; this model has the same total charge as the AIMD-c charge but a different distribution.

2. METHODOLOGY AND SIMULATION DETAILS

2.1. Derivation of Atomic Charges. The atomic charge was derived from AIMD calculations. The unit cells of [BMIM][PF6] and [EMIM][PF6] crystal structures,[1,78]

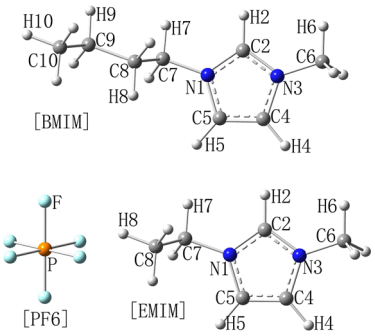

Figure 1. Atomic labeling in $[BMIM]^+$, $[EMIM]^+$, and $[PF6]^-$, respectively.

containing two and four ion pairs, respectively, were simulated using the package CPMD.[79] The PBE functional[80,81] was used with the norm conserving pseudopotential of the Troullier−Martins form.[82] The wave functions were optimized every step (BOMD) with convergence criteria of 10^{-7}. The time step of 4 au (around 0.096 fs) was used, and the energy cutoff was set to 90 Ry. The crystal structure was briefly equilibrated for 1000 steps at 300 K. A simulated annealing was then carried out, and the crystal structure was quenched to the potential energy minimum within 3000 steps. The atomic charges were then derived by fitting the DFT electrostatic potential surface using the ESP method[83] implemented in CPMD. The charges thus obtained were averaged over ion pairs within the unit cell, two for [BMIM][PF6] and four for [EMIM][PF6], respectively, and the equivalent atoms within the ion pair (for example, six F's of [PF6] or three H's on a methyl group). The total charge on each ion was found to be ±0.8 for both ionic liquids. These charges will be referred to as "AIMD-c charges".

For comparison purposes, another set of atomic charges was obtained following a conventional procedure. Structures of the isolated ions, [BMIM], [EMIM], and [PF6], were optimized in a vacuum at the B3LYP/6-311++G(d,p) level using the Gaussian 09 package.[84] The atomic charges were derived using the RESP method.[85] This set of charges has unit total charge on the cation and anion, respectively, and is denoted as "full charge".

The third set of atomic charges was obtained by scaling the full charges uniformly by a factor of 0.8, to agree with the total charges derived from the above AIMD simulations. Note that the charge distributions are different for these "scaled charges" and the AIMD-c charges.

Two more sets of atomic charges were derived from liquid phase AIMD simulations. The simulation box containing eight pairs of [BMIM][PF6] or [EMIM][PF6], mimicking their liquid phases,[76] was first equilibrated with a classical force field for 2 ns in a constant volume and constant temperature (NVT) ensemble. The size of the simulation box was chosen so that the system density agreed with the experimental value. A Car−Parrinello type dynamics was then carried out using the package CPMD.[79] The same DFT functional and pseudopotential as in the AIMD-c case was used. A trajectory of about 6 ps was generated for each system with a time step of 4 au. The first ps of the trajectory was considered as equilibration, and snapshots were taken from the remaining 5 ps every 1000 steps. Atomic charges were derived from each of the 50 configurations by fitting the electrostatic potential surface using the ESP method and averaging over equivalent atoms. This set of atomic charges is hereafter referred to as "AIMD-l" charge. Using the

dx.doi.org/10.1021/jp3037999 | J. Phys. Chem. B 2012, 116, 10036−10048

same configurations, the atomic charges were also derived using the Blöchl approach[86] implemented in the package CP2K,[87] following the procedure developed by Delle Site and co-workers.[77] Different from Delle Site's work, the PBE functional and TZV2P basis sets and Goedecker–Teter–Hutter form of the pseudopotential[88,89] were used in the current study. This set of atomic charges is referred to as "AIMD-b" charge.

A summary of the methods used to obtain the five sets of atomic charges is given in Table 1. The BOMD method has been used in the derivation of AIMD-c charges in the current work. CPMD can be used as well which was found to result in the same partial charges. Computationally, the derivation of the AIMD-l and AIMD-b charges is potentially at least 40 times more expensive than that of AIMD-c charges.

Table 1. Summary of the Atomic Charge Derivation Details

	system	environment	method
full charge	isolated ion	vacuum	RESP
scaled charge	isolated ion	vacuum	RESP/scaled
AIMD-c charge	2 or 4 IL pairs	crystal/periodic	ESP
AIMD-l charge	8 IL pairs	liquid/periodic	ESP
AIMD-b charge	8 IL pairs	liquid/periodic	Blöchl

2.2. Molecular Dynamics Simulations. The general Amber force field (GAFF)[90] was used with the five sets of atomic charges in the current study. The P–F bond parameters were taken from ref 42. Classical molecular dynamics (MD) simulations were carried out in the isothermal–isobaric (NPT) and canonical (NVT) ensembles using the LAMMPS package[91] with periodic boundary conditions. A time step of 1 fs was used. The long-range electrostatic interactions were calculated using the Ewald/n method[92] with a real space cutoff of 12 Å. The Nosé–Hoover thermostat[93] and the extended Lagrangian approach[94] were applied to control the temperature and pressure, respectively. The pressure was fixed to be 1 atm in all constant pressure simulations with isotropic volume fluctuations for the liquid phase and anisotropic cell for the crystal phase.

The crystal phases of the simulation systems were built up by reproducing the corresponding crystal unit cell by 5, 5, and 5 in the *X*, *Y*, and *Z* directions, respectively, for [BMIM][PF6] and 5, 5, and 4 for [EMIM][PF6]. A total of 250 and 400 ion pairs were included in the simulation box for [BMIM][PF6] and [EMIM][PF6], respectively. The liquid phase systems were initially prepared by putting the same number of ion pairs (250 for [BMIM][PF6] and 400 for [EMIM][PF6], respectively) randomly in a cubic box. The systems were then equilibrated for 2 ns in the NPT ensemble followed by 20 ns production runs in the NVT ensemble. The last 15 ns of the NVT trajectories were used for analysis.

2.3. Pseudosupercritical Path (PSCP) Method. The recently revised PSCP procedure[95] was applied in the current work for the calculation of melting points. The procedure includes two steps. In the first step, the free energy of pure liquid and pure solid phases as a function of temperature were calculated from a series of constant pressure and constant temperature (*NPT*) simulations based on the Gibbs–Helmholtz equation

$$\frac{G}{RT} - \left(\frac{G}{RT}\right)_{\mathrm{ref}} = \int_{T_{\mathrm{ref}}}^{T} -\frac{H}{RT^2}\,\mathrm{d}T \tag{1}$$

where T_{ref} is an arbitrary reference temperature and H is the enthalpy.

The absolute free energy difference ΔG between the liquid (L) and crystal (C) phases at the reference temperature was then determined in the second step using the thermodynamic integration method along a reversible pseudosupercritical path (PSCP). Along the PSCP path, the liquid and crystal phases are connected by three intermediate states, the weakly interacting liquid (WL), the dense weak fluid (DWF), and the weakly interacting crystal (WC).[95]

The calculation of ΔG along the PSCP path starts with the crystal phase. In the first step, the WC state is accomplished by scaling down the intermolecular potential energy based on the following equation:

$$U(\lambda) = [1 + \lambda(\eta - 1)]^m U^{\mathrm{vdW}} + [1 + \lambda(\eta - 1)]^n U^{\mathrm{elec}} \tag{2}$$

where U^{vdW} and U^{elec} are the van der Waals and electrostatic components of the potential energy, respectively, η is a scaling parameter having a value of $0 < \eta < 1$, m and n are positive integer exponents, and λ is a coupling parameter that ranges from 0 to 1. Simultaneously, a tethering potential of the form

$$U_{\mathrm{tether}} = -\lambda \sum_i \sum_j a_{ij} \exp(-b_{ij} r_{ij}^{\,2}) \tag{3}$$

is turned on so that the crystalline order is retained during this step. Again, λ starts at 0 and ends at 1 during this step. The positions of these Gaussian wells are based on the average particle coordinates in the crystal phase. The well depth and width are controlled by parameters a_{ij} and b_{ij} so that the atoms under the tethering potential experience the same thermal fluctuations as in the crystal phase. The free energy changes associated with this step are calculated via thermodynamic integration:

$$\Delta A = \int_0^1 \left\langle \frac{\partial U}{\partial \lambda} \right\rangle_\lambda \mathrm{d}\lambda \tag{4}$$

where $U = U(\lambda) + U_{\mathrm{tether}}$.

In the second step along the PSCP path, the external tethering potential is gradually turned off

$$U(\lambda) = -(1 - \lambda) \sum_i \sum_j a_{ij} \exp(-b_{ij} r_{ij}^{\,2}) + U^{\mathrm{NS}} \tag{5}$$

where U^{NS} denotes all potential energy terms that are not scaled or affected. The crystal structure of the weakly interacting system breaks down in this step in a controlled manner, and the error associated with superheating is minimized.[95]

In the third step along the path, the box size is changed from the average crystal phase volume V^{C} to the average liquid phase volume V^{L} at the reference temperature. The corresponding free energy change is given by

$$\Delta A = \int_{V^{\mathrm{L}}}^{V^{\mathrm{C}}} -\langle P \rangle\, \mathrm{d}V \tag{6}$$

In the last step, the intermolecular potential is restored on the basis of the following expression

$$U(\lambda) = [\eta + \lambda(1 - \eta)]^m U^{\mathrm{vdW}} + [\eta + \lambda(1 - \eta)]^n U^{\mathrm{elec}} \tag{7}$$

At the end of this step, the liquid phase is obtained. The Helmholtz free energy change associated with this step and the second step can be computed using eq 4. The sum of the free energy change from all four steps corresponds to the free

dx.doi.org/10.1021/jp3037999 | J. Phys. Chem. B 2012, 116, 10036–10048

energy difference between the crystal and liquid phases at the reference temperature.

The free energy curves for the single phase systems were generated from NPT ensemble simulations. A 2 ns trajectory was generated at each temperature, and the last 1 ns was used for analysis. In each step along the PSCP path, in order to compute the free energy change using the thermodynamic integration method, $\langle \partial U/\partial \lambda \rangle_\lambda$ or $\langle P \rangle$ was calculated with nine λ values or box volumes in addition to initial and final states. A 2 ns NVT ensemble simulation at a reference temperature of 340 K for [BMIM][PF6] and 380 K for [EMIM][PF6] was carried out at each λ or V value, and the last 1 ns was used for analysis. Parameters m, n, and η were chosen as 1, 2, and 0.1, respectively.[96]

3. RESULTS AND DISCUSSION

3.1. Atomic Charges. The five sets of atomic charges derived in the current work are shown in Figure 2, and the total charges on each ion are summarized in Table 2. Atomic labels follow those in Figure 1. As shown in Table 2, the total charge was found to be ±0.80 e for both [BMIM][PF6] and [EMIM][PF6] using the AIMD-c procedure and ±0.85 e using the AIMD-l procedure. The AIMD-b procedure yielded slightly different total charges for the two ILs, ±0.80 e for [BMIM][PF6] and ±0.76 e for [EMIM][PF6], respectively.

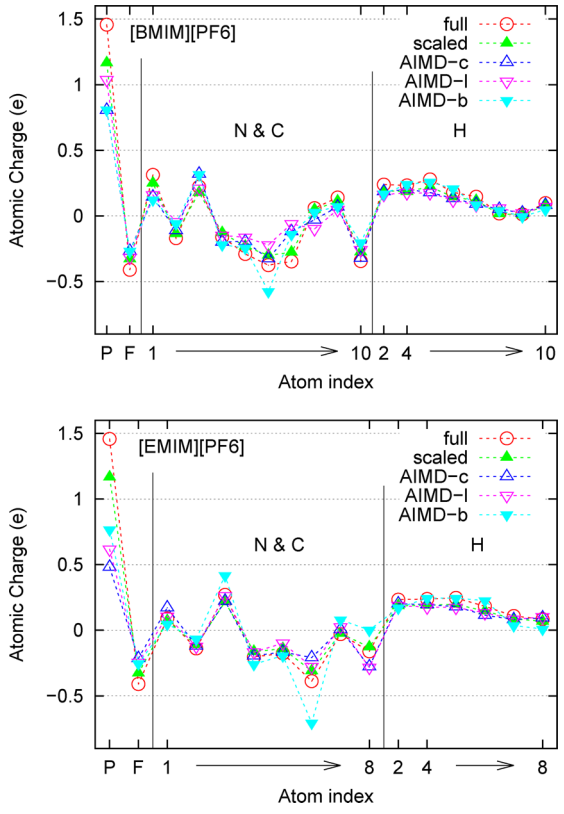

Figure 2. The five sets of atomic charges applied in the current work. The "full charge" was derived using the RESP method[85] from isolated ion in a vacuum at the B3LYP/6-311++G(d,p) level and has the total charge of unity, the "scaled charge" was obtained by uniformly scaling the "full charge" by a factor of 0.8, and the "AIMD-c charge" was derived using the ESP method[83] from the periodic crystal phase AIMD simulation. The "AIMD-c charge" has a total charge of ±0.8 e on the cation and anion, respectively, but the charge distribution is different from "scaled charge". The "AIMD-l" and "AIMD-b" charges were based on liquid phase AIMD simulations and used the ESP method and Blöchl method, respectively.

Table 2. Summary of Total Charges (in e) on Each Ion Derived Using Different Methods

	[BMIM][PF6]	[EMIM][PF6]
full charge	±1.00	±1.00
scaled charge	±0.80	±0.80
AIMD-c charge	±0.80	±0.80
AIMD-l charge	±0.85	±0.85
AIMD-b charge	±0.80	±0.76

As shown in Figure 2, the five sets of charges were found to be similar. The largest deviation was observed for the P atom in the anion, which also has the largest absolute value. When derived from an isolated ion in a vacuum, the P atom was found to have a charge of +1.46 e. When scaled, it becomes +1.17 e, whereas AIMD methods yield a charge of +0.81 e (AIMD-c), +1.04 e (AIMD-l), and +0.81 e (AIMD-b) for [BMIM][PF6], respectively, and +0.48 e (AIMD-c), +0.62 e (AIMD-l), and +0.77 e (AIMD-b) for [EMIM][PF6], respectively. Another significant deviation was observed for C6 atoms which were found to have more negative charges from the AIMD-b procedure for both ILs, consistent with earlier results.[75]

The two ILs have similar cations (in terms of their formula) and share the same anion [PF6]. However, the crystal structures of the two ILs belong to different space groups and obey different symmetries.[1,78] As a result, the charges on P and F atoms are quite different due to the differences in their local environments. The absolute values of charges for both P and F are smaller when [PF6] is paired with [EMIM], consistent with the fact that [EMIM] has a shorter hydrophobic alkyl chain and so the system likely exhibits more charge transfer than [BMIM][PF6]. This effect cannot be captured if charges are developed for isolated ions. By developing partial charges from condensed phase simulations, it is hoped that a better representation of the "true" charge distribution is obtained. The same general Amber force field was applied with each set of charges, and the impact of these different charge distributions on physical properties is reported below.

3.2. Density. The crystal phase of both ionic liquids was simulated using the five sets of atomic charges at 173 K, the temperature at which the crystal structure was measured. The crystal structures were found to be stable in all cases, and the equilibrium lattice parameters are summarized in Table 3. All five sets of atomic charges predicted similar lattice parameters and agree well with experimental results.[1,78] For both ionic liquids, the full charge predicted the highest densities, which are 4.9% and 2.5% lower than the experimental results, respectively. For [BMIM][PF6], all three sets of AIMD charges generated slightly lower densities than the full charge, followed by the scaled charge result, which is 6.3% lower than experimental densities. For [EMIM][PF6], the calculated densities were found to be similar for the scaled charges and AIMD-b charges, although the latter has smaller total charge. The densities calculated using the other two sets of AIMD charges were found to be similar in spite of the difference in total charges.

The liquid phase densities of the two ionic liquids were computed as a function of temperature. The results are shown in Figure 3. The computed densities using all five sets of charges are within 6% of the experimental results.[97,98] The full charge results perfectly reproduced experimental densities for both ionic liquids, whereas the scaled charges and AIMD

dx.doi.org/10.1021/jp3037999 | J. Phys. Chem. B 2012, 116, 10036−10048

Table 3. Calculated Lattice Parameters and Density for [BMIM][PF6] and [EMIM][PF6] at 173 K Compared with Experimental Results (Length in Å and Angle in deg)

	a	b	c	α	β	γ	density (g/cm^3)
				[BMIM][PF6]			
full charge	9.083	9.039	8.999	95.91	114.99	102.86	1.484
scaled charge	9.091	9.068	9.079	95.88	114.76	102.82	1.461
AIMD-c charge	9.015	9.044	9.091	95.85	114.72	102.85	1.475
AIMD-l charge	9.042	9.040	9.055	95.87	114.83	102.86	1.479
AIMD-b charge	9.045	9.021	9.106	95.83	114.68	102.89	1.471
Exp.	8.755	8.904	9.013	95.81	114.95	103.06	1.560
				[EMIM][PF6]			
full charge	8.633	9.202	13.555	90.00	101.84	90.00	1.615
scaled charge	8.710	9.224	13.713	90.00	101.71	90.00	1.578
AIMD-c charge	8.680	9.102	13.805	90.00	101.63	90.00	1.593
AIMD-l charge	8.671	9.105	13.767	90.00	101.66	90.00	1.599
AIMD-b charge	8.679	9.185	13.825	90.00	101.61	90.00	1.577
Exp.	8.627	9.035	13.469	90.00	101.92	90.0	1.656

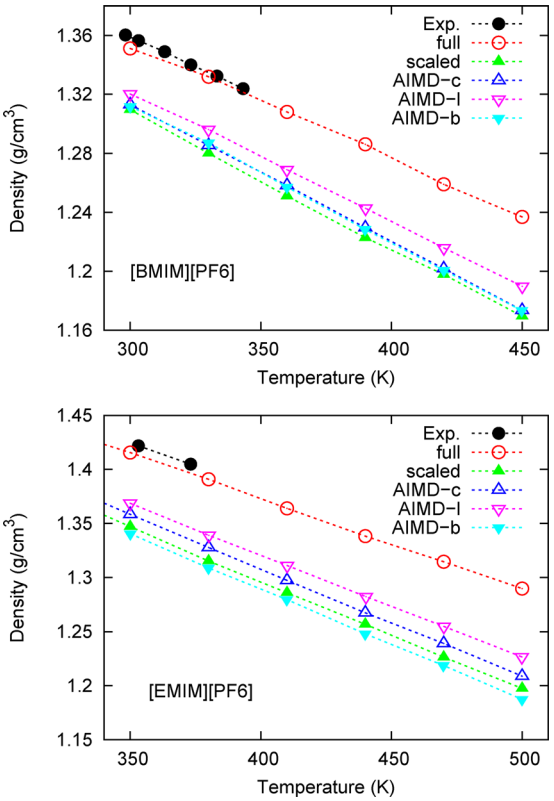

Figure 3. The liquid phase density as a function of temperature computed with the five sets of atomic charges for [BMIM][PF6] (top) and [EMIM][PF6] (bottom). Experimental values were taken from refs 97 and 98. The calculated results using full charge agree well with experimental results, whereas the reduced charges underestimate the liquid density but are still within 6% of the experimental results.

charges predicted lower densities, similar to the lattice phase results. This is due to the fact that the intermolecular electrostatic interactions are weakened with reduced charges. The differences in predicted densities by the four sets of reduced charges are within 2% of each other.

3.3. Liquid Phase Structure. The liquid phase structure of both ionic liquids was studied in terms of radial distribution functions (RDFs). The center of mass RDFs computed at 360 K for [BMIM][PF6] and 410 K for [EMIM][PF6], respectively, are shown in Figure 4. The results at other temperatures show similar behavior.

For [BMIM][PF6], the cation−anion RDFs show a sharp peak at about 5.0 Å and a shoulder at ∼6.8 Å, indicating a well-organized liquid structure. Due to the long-range electrostatic interaction, the ordered structure was observed for up to 20 Å. With reduced charges, the height of the first peak decreased slightly and the shoulder structure at 6.8 Å became less clear, consistent with previous observation that the liquid phases of ILs are less structured when simulated using reduced atomic charges.[72] The coordination number in the first solvation shell was computed by integrating the RDFs to the first minimum at about 8.5 Å in g_{+-} and between 11−13 Å in g_{++} and g_{--}. The results are summarized in Table 4. The cation−anion coordination number was found to be about 7.0 for all five sets of atomic charges in spite of the slightly different packing structures.

Because of the different packing structures between cations and anions, the cation−cation and anion−anion RDFs show differences when simulated using different charges. Interestingly, the relative heights of the split peaks of the first solvation shell in the anion−anion RDF, which is associated with different binding positions of the anions around cations, switched when the charges were reduced, although the coordination numbers are still similar, as shown in Table 4. The coordination number using AIMD-l charges was found to be lower than the results using other sets of charges.

The results for [EMIM][PF6] show similar behavior. The ethyl group in the [EMIM] cation is shorter than the butyl group in the [BMIM] cation, and as a result, the coordination numbers were found to be larger in the case of [EMIM][PF6].

The liquid phase structures of both ionic liquids were further studied by spatial distribution functions (SDFs). The anion center of mass distributions around cations are shown in Figures 5 and 6 for [BMIM][PF6] and [EMIM][PF6], respectively. As reported previously,[38,42] the anions have three preferred binding positions around the cations, located around H2, H4, and H5 atoms, respectively. The area around the H2 atom was found to be the most favorable region. Due to the repulsion from the butyl or ethyl chain, the anion distribution was pushed to the methyl side in both ILs. The distribution probability around the H4 atom is lower than that around the H5 atom for the same reason. When the atomic charges are reduced, the iso-density surface around the H2

dx.doi.org/10.1021/jp3037999 | J. Phys. Chem. B 2012, 116, 10036−10048

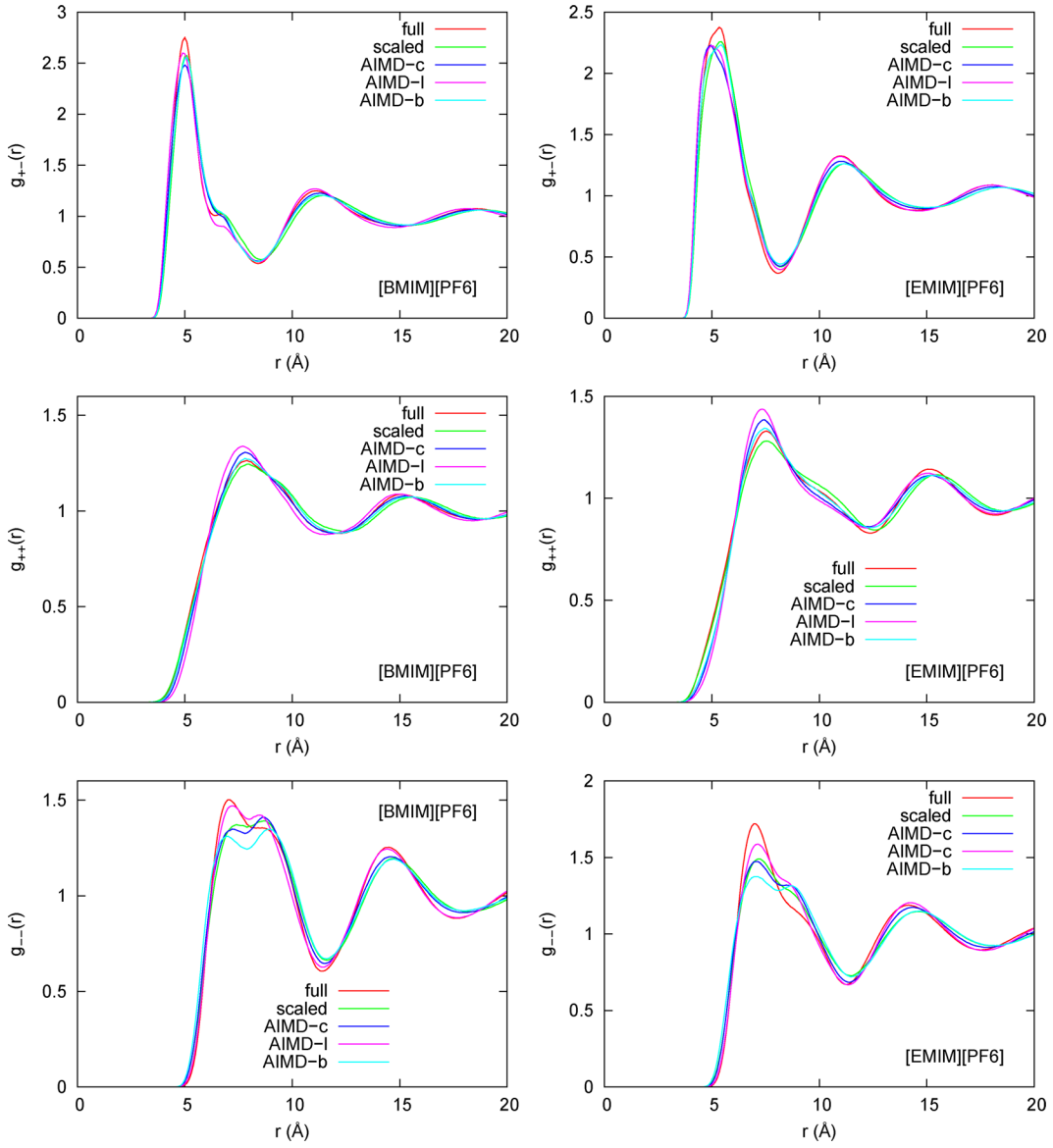

Figure 4. The center of mass radial distribution function derived from 15 ns NVT ensemble simulations for [BMIM][PF6] at 360 K and for [EMIM][PF6] at 410 K using the five sets of atomic charge parameters. The coordination number in the first solvation shell was computed by integrating the RDF curves to the first minimum, and the results are summarized in Table 4. Results at other temperatures show similar behavior.

Table 4. Calculated Coordination Number in the First Solvation Shell of Liquid [BMIM][PF6] at 360 K and [EMIM][PF6] at 410 K

	cation−anion	cation−cation	anion−anion
	[BMIM][PF6]		
full charge	6.9	19.8	16.6
scaled charge	7.0	20.9	16.7
AIMD-c charge	6.7	18.2	16.4
AIMD-l charge	6.8	16.5	16.0
AIMD-b charge	6.7	19.5	16.8
	[EMIM][PF6]		
full charge	7.4	24.3	18.3
scaled charge	7.3	24.1	18.3
AIMD-c charge	7.2	23.1	18.0
AIMD-l charge	7.2	22.7	18.0
AIMD-b charge	7.2	22.8	18.3

atom becomes narrower and further extended to above and below the imidazolium ring. The distribution probability around H4 and H5 atoms was found to decrease due to the weaker interaction between the cation and anion. In spite of such reorganization in packing structure, the cation−anion coordination numbers are still about the same with all five sets of atomic charges. These results suggest that the overall local structure, as characterized by RDFs and SDFs, is insensitive to the way in which partial charges are determined.

3.4. Mean Squared Displacement and Self-Diffusivity.

On the basis of 15 ns NVT trajectories, the translational properties of the ionic liquids were quantified in terms of the mean-square displacements (MSDs) of the ion center of mass:

$$\mathrm{MSD}(t) = \langle (r_i(t) - r_i(0))^2 \rangle \tag{8}$$

where $r_i(t)$ is the center of mass of ion i at time t. Figure 7 shows the MSDs calculated for [BMIM][PF6] at 360 K and [EMIM][PF6] at 410 K, respectively. Results at other

dx.doi.org/10.1021/jp3037999 | J. Phys. Chem. B 2012, 116, 10036−10048

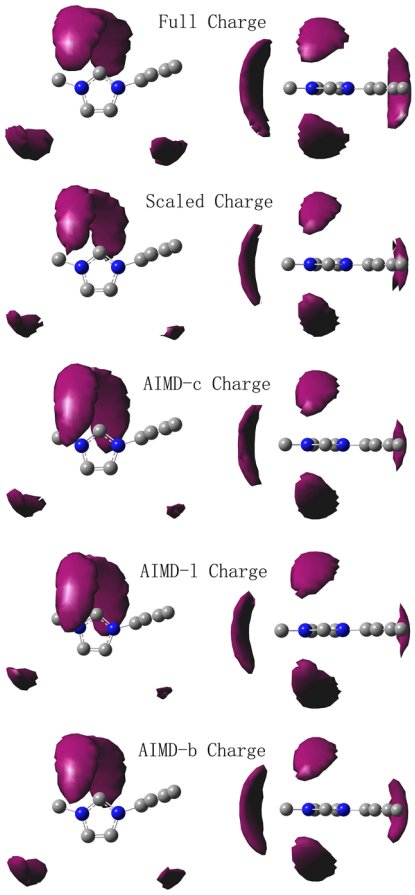

Figure 5. The spatial distribution function for anion around cation in liquid [BMIM][PF6] at 360 K derived from 15 ns NVT simulation (left, side view; right, top view). The iso-density surface was drawn at 10 times the average density. Anions were found to have preferred distribution around H2, H4, and H5 atoms with all five sets of atomic charges. The distributions around H4 and H5 were smaller for the reduced charges. Results at other temperatures show a similar trend.

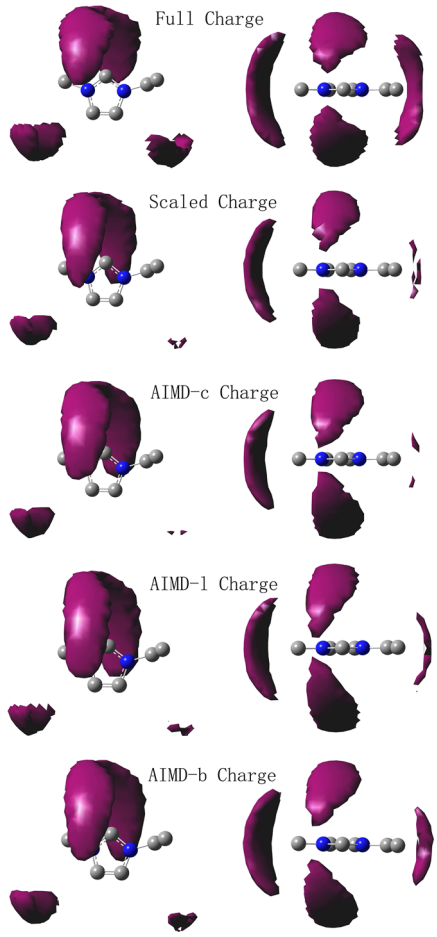

Figure 6. The spatial distribution function for anion around cation in liquid [EMIM][PF6] at 410 K derived from 15 ns NVT simulation (left, side view; right, top view). The iso-density surface was drawn at 7 times the average density. Anions were found to have preferred distribution around H2, H4, and H5 atoms with all five sets of atomic charges. The distributions around H4 and H5 were smaller for the reduced charges. Results at other temperatures show a similar trend.

temperatures show a similar trend. For both ionic liquids, the dynamics of the ions are significantly increased when reduced charges are used. In all cases, the cations were found to translate faster than the anions, although the anions are smaller.

The self-diffusion coefficients can be computed from the MSD using the Einstein relation:

$$D_s = \frac{1}{6}\lim_{t\to\infty}\frac{d}{dt}\langle(r_i(t) - r_i(0))^2\rangle \quad (9)$$

The slope of the MSD versus time in the normal diffusion region (see Figure 8) was used to estimate the self-diffusivity in each case, and the results are shown in Figure 9. In [BMIM][PF6], relative to experimental results, the ion diffusion was significantly underestimated by the full charges. With both scaled and AIMD-c charges, experimental self-diffusivities[99] for both cation and anion are reproduced very well. The difference between the scaled charges, AIMD-c charges, and AIMD-b charges, all having a total charge of ±0.80 e, are up to 50%, indicating that the dynamic properties of ionic liquids are much more sensitive to the distribution of charges than are static properties such as density, consistent with previous studies.[100,11] AIMD-l charges, having larger total charges on each ion (±0.85 e), predicted slower dynamics than other reduced charges. The self-diffusion coefficients derived from simulations using AIMD-l charges are about half of the experimental results. Experimental diffusivity results are not available for [EMIM][PF6], but the computed results from the five sets of charges follow a similar trend as [BMIM][PF6].

3.5. Rotational Dynamics. The rotational dynamics of the ions were studied from the correlation function[101] defined as

$$C(t) = \left\langle \frac{1}{2}[3\cos^2\theta_i(t) - 1] \right\rangle \quad (10)$$

where θ is the angle between a given vector at time t and time zero. Three perpendicular vectors are considered for the cations in the current work. The first vector is along the line connecting the two nitrogen atoms of the imidazolium ring, the second vector is defined by the line that passes through the C2 atom and is perpendicular (and intersects) with the first vector, and the third vector is normal to the plane defined by the first two vectors (cross product of the first two vectors). A typical correlation function is shown in Figure 10. The rotational correlation time constant, τ, was calculated by the following integration:

$$\tau = \int_0^\infty C(t)\,dt \quad (11)$$

dx.doi.org/10.1021/jp3037999 | J. Phys. Chem. B 2012, 116, 10036−10048

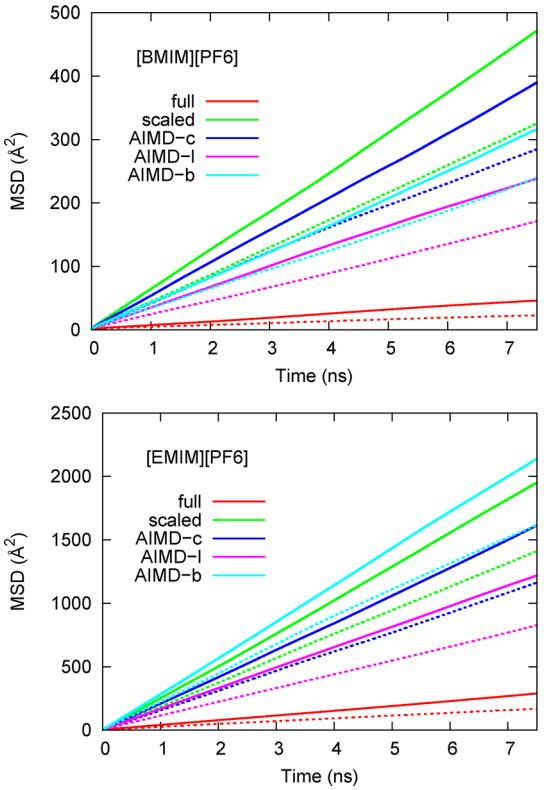

Figure 7. The computed center of mass (solid lines, cation; dashed lines, anion) mean square displacement in liquid [BMIM][PF6] at 360 K (top) and [EMIM][PF6] at 410 K (bottom). The ion center of mass dynamics were significantly accelerated by the reduction of charges on the atoms. Results at other temperatures show a similar trend.

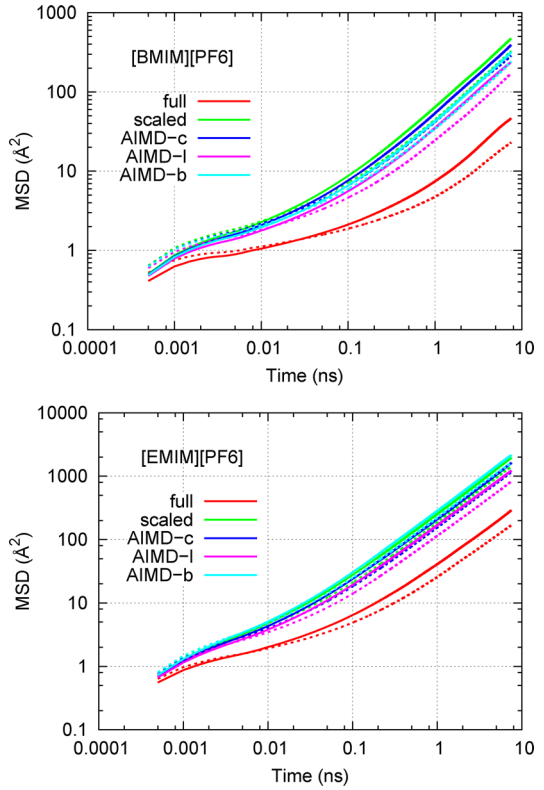

Figure 8. The computed center of mass (solid lines, cation; dashed lines, anion) mean square displacement in liquid [BMIM][PF6] at 360 K (top) and [EMIM][PF6] at 410 K (bottom) in log~log scale. The slope approaches unity at long time, indicating normal diffusion motion.

where $C(t)$ was fit to a stretched exponential function of the form

$$C(t) = a_0 e^{-(t/\tau_0)^{\beta}} \tag{12}$$

where a_0 is a constant, τ_0 is the rotational time constant, and β is a stretching parameter that has values between 0 and 1. Materials with β values significantly below unity are indicative of glasses.[102] Table 5 summarized the fitting coefficients to eq 12 for [BMIM] and [EMIM], respectively. The computed rotational correlation time constants are summarized in Table 6.

The vector connecting the two ring nitrogen atoms (vector 1) roughly aligns with the alkyl chains in the cation and represents the largest molecular extent. As expected, the slowest relaxation was observed for this vector in both ionic liquids, independent of the atomic charges. For a given vector, the rotational correlation time constants are predicted to be several times larger for the full charge case relative to the reduced charge results, indicating faster rotational dynamics in the reduced charges simulations. Similar to the results of translational diffusivities, the differences among the reduced charges are up to 45%. In spite of the large difference in the correlation time constants, the fitted stretching parameters, β, were found to be similar in all cases. The translational and rotational dynamics results indicate that the use of integer charges severely underestimates the translational and rotational dynamics of ILs. Scaling the charges uniformly improves the dynamics without perturbing the local structure to a great extent. The charge distribution is also important, however, such that the dynamics obtained with scaled charges or AIMD charges are still significantly different from each other.

3.6. Ionic Conductivity. The ionic conductivity were calculated using the Nernst−Einstein (NE) equation:

$$\sigma_{NE} = \frac{N_{pair}}{Vk_BT}(q_+{}^2D_+ + q_-{}^2D_-) \tag{13}$$

where N_{pair} is the number of ion pairs, V the simulation box volume, k_B the Boltzmann constant, and T the temperature. q_+ and q_- are the total charges of the ions, as summarized in Table 2, and D_+ and D_- are the self-diffusivities of the cation and anion, respectively. The calculated results are shown in Figure 11. Similar to self-diffusivities, the calculated ionic conductivities for [BMIM][PF6] using the scaled charge or AIMD-c charges agree with experimental results very well. AIMD-l and AIMD-b charges slightly underestimate the ionic conductivities, especially at low temperatures. Significant errors were observed in results using the full charge.

The ionic conductivity can also be calculated using the following Einstein expression:

$$\sigma_E = \frac{1}{6k_BTV}\lim_{t\to\infty}\frac{d}{dt}\langle\sum_{i=1}^{N}\sum_{j=1}^{N}q_iq_j[r_i(t) - r_i(0)]\cdot [r_j(t) - r_j(0)]\rangle \tag{14}$$

It is clear from eq 14 that the correlation term, ignored by the simple Nernst−Einstein model, is included here. However,

dx.doi.org/10.1021/jp3037999 | J. Phys. Chem. B 2012, 116, 10036−10048

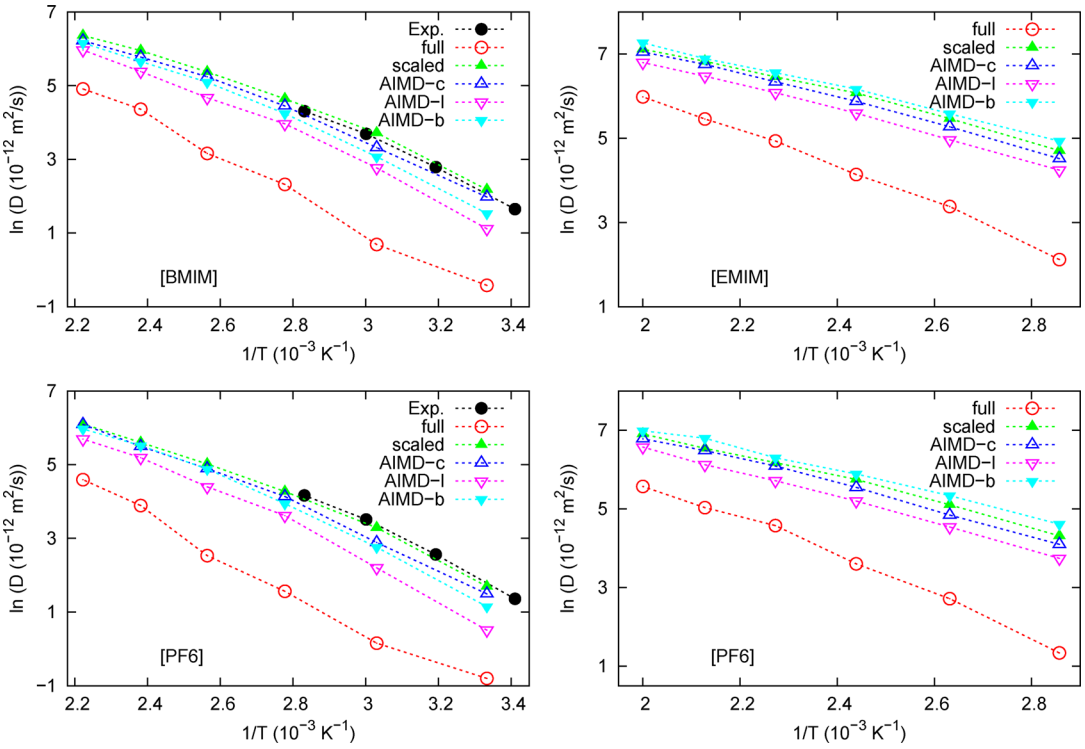

Figure 9. The ion self-diffusion coefficients derived on the basis of the Einstein relation for [BMIM][PF6] and [EMIM][PF6], respectively. The experimental results for [BMIM][PF6] were taken from ref 99. The calculations using the AIMD-c or scaled atomic charges reproduce experimental results very well.

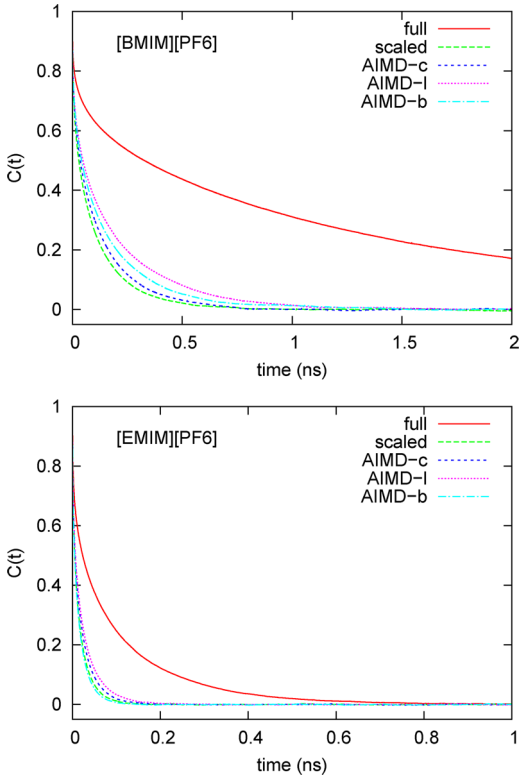

Figure 10. The computed rotational correlation function for the vector connecting the two nitrogen atoms in the cation (vector 1) for [BMIM][PF6] at 360 K (top) and [EMIM][PF6] at 410 K (bottom). The reduced charges predicted significantly faster relaxation of rotational correlation for both ionic liquids. Results for the other two vectors as well as other temperatures show a similar trend.

even longer trajectories are likely needed to get accurate results. This method was not applied in the current work.

3.7. Phase Change Enthalpy. The vaporization enthalpy (ΔH_v) and fusion enthalpy (ΔH_f) were computed for both ionic liquids using the five sets of atomic charges. The results are summarized in Table 7. For both ionic liquids, the computed vaporization enthalpies using reduced charges are similar to each other and are lower than the full charge results. Experimental values are not available in the literature for these two compounds. A recent prediction[103] based on experimental results of similar ILs suggested that ΔH_v = 37.53 kcal/mol for [BMIM][PF6] and ΔH_v = 38.24 kcal/mol for [EMIM[PF6], which are close to the values obtained in the current study. It is worth noting that the vaporization enthalpy was calculated in the current work using the same force field for the liquid phase and gas phase. Because the charge transfer and polarization properties are different in the two phases, strictly speaking, a separate set of charges should be developed for the gas phase simulation; the current results should be considered as a rough estimation.

The fusion enthalpy of both ionic liquids was computed, and the results are shown in Table 7. For both ionic liquids, the fusion enthalpies ΔH_f calculated using the AIMD-c charges are in good agreement with experimental results,[104] indicating that the AIMD-c charges describe both the crystal and liquid phases properly. Using the scaled charges or other AIMD charges derived from liquid phase simulations, the fusion enthalpy was significantly underestimated. For the full charge, the calculated fusion enthalpy was underestimated in the [BMIM][PF6] case, whereas it was overestimated for [EMIM][PF6].

3.8. Melting Points. Using the recently revised PSCP method,[95] the normal melting temperatures were calculated for [BMIM][PF6] and [EMIM][PF6] and the results are

dx.doi.org/10.1021/jp3037999 | J. Phys. Chem. B 2012, 116, 10036−10048

Table 5. Coefficients (Time in ns) Fitted to eq 12 for the Rotational Dynamics of the Cation in Liquid [BMIM][PF6] at 360 K and [EMIM][PF6] at 410 K[a]

	vector 1			vector 2			vector 3		
	a_0	τ_0	β	a_0	τ_0	β	a_0	τ_0	β
				[BMIM][PF6]					
full charge	0.751	1.157	0.759	0.623	0.657	0.650	0.643	0.801	0.624
scaled charge	0.851	0.077	0.683	0.852	0.024	0.497	0.825	0.032	0.519
AIMD-c charge	0.835	0.096	0.710	0.813	0.031	0.528	0.786	0.042	0.554
AIMD-l charge	0.821	0.144	0.678	0.794	0.043	0.506	0.769	0.064	0.524
AIMD-b charge	0.836	0.116	0.684	0.787	0.047	0.537	0.751	0.064	0.583
				[EMIM][PF6]					
full charge	0.819	0.074	0.661	0.840	0.022	0.479	0.730	0.055	0.559
scaled charge	0.952	0.011	0.642	0.995	0.003	0.500	0.963	0.005	0.482
AIMD-c charge	0.933	0.014	0.648	0.987	0.004	0.494	0.946	0.006	0.486
AIMD-l charge	0.929	0.016	0.630	0.989	0.004	0.476	0.943	0.007	0.464
AIMD-b charge	0.949	0.010	0.663	0.988	0.003	0.522	0.962	0.005	0.502

[a]See text for the definition of the three vectors.

Table 6. Calculated Rotational Correlation Time Constants (ns) for the Cation in Liquid [BMIM][PF6] at 360 K and [EMIM][PF6] at 410 K[a]

	vector 1	vector 2	vector 3
	[BMIM][PF6]		
full charge	1.024	0.560	0.739
scaled charge	0.086	0.042	0.050
AIMD-c charge	0.100	0.047	0.056
AIMD-l charge	0.155	0.068	0.091
AIMD-b charge	0.126	0.066	0.075
	[EMIM][PF6]		
full charge	0.082	0.042	0.067
scaled charge	0.016	0.009	0.013
AIMD-c charge	0.019	0.010	0.014
AIMD-l charge	0.022	0.011	0.017
AIMD-b charge	0.014	0.009	0.012

[a]See text for the definition of the three vectors.

summarized in Table 8. For both ILs, the full charges overestimate the experimental melting temperature,[1,78] whereas the scaled charges underestimate the melting temperature. Using the AIMD-c charges, the melting temperature was predicted to be 284 K for [BMIM][PF6] and 330 K for [EMIM][PF6], respectively, in excellent agreement with experimental values of 284 and 338 K, respectively. AIMD-l charges successfully predicted the melting point of [EMIM][PF6] but failed in the case of [BMIM][PF6]. AIMD-b charges overestimated the melting point of [BMIM][PF6] and underestimated that of [EMIM][PF6]. The improved performance of the AIMD-c charges relative to the other charges for predicting melting point is consistent with the fusion enthalpy calculations, indicating the reliability of the AIMD-c charges in predicting the phase change behavior of both ionic liquids.

As mentioned earlier, the PSCP method is a free energy based method. The computed free energy differences (ΔG) at the reference temperature are provided in Table 9, and the free energy curves used to obtain the melting temperatures are shown in Figure 12 for each case. The free energy curves in Figure 12 are sharper for the full charge calculation, although the free energy differences between the liquid and crystal phases are similar in each case. It was pointed out previously[96] that the calculated melting temperature using the PSCP method highly depends on the accuracy of ΔG. By comparing

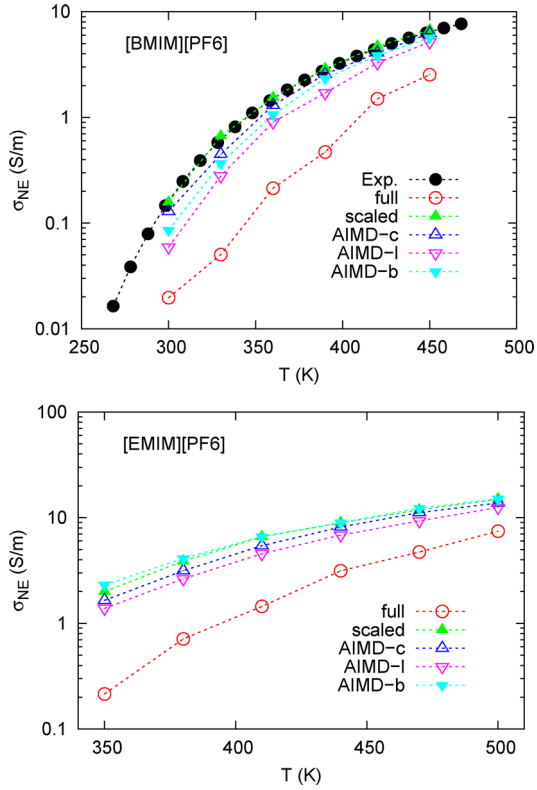

Figure 11. The ionic conductivities derived from the Nernst−Einstein relation for [BMIM][PF6] (top) and [EMIM][PF6] (bottom), respectively. The experimental results for [BMIM][PF6] were taken from ref 106. The calculated σ_{NE} using AIMD-c or scaled charges reproduce experimental results very well.

Tables 8 and 9, it can be seen that the small difference in ΔG can cause a large deviation in the predicted melting temperature.

4. CONCLUDING REMARKS

We have presented a way of deriving atomic charges by using density functional theory and plane wave basis set calculations on the crystal phase of ionic liquids. This approach is similar to previous efforts[75−77] where AIMD was run on the liquid phase. The advantage of the present method is that extensive sampling of configurational space in the liquid phase simulation is

dx.doi.org/10.1021/jp3037999 | J. Phys. Chem. B 2012, 116, 10036−10048

Table 7. Calculated Vaporization Enthalpy (ΔH_v) and Fusion Enthalpy (ΔH_f) for [BMIM][PF6] (298 and 284 K, Respectively) and [EMIM][PF6] (298 and 334 K, Respectively) (Units: kcal/mol)

	ΔH_v	ΔH_f
	[BMIM][PF6]	
full charge	44.99 ± 0.18	3.93 ± 0.04
scaled charge	34.68 ± 0.16	2.99 ± 0.04
AIMD-c charge	34.18 ± 0.18	4.50 ± 0.04
AIMD-l charge	34.56 ± 0.17	3.75 ± 0.04
AIMD-b charge	34.08 ± 0.18	4.40 ± 0.04
Exp.	37.53[a]	4.76[b]
	[EMIM][PF6]	
full charge	45.85 ± 0.14	4.61 ± 0.03
scaled charge	34.60 ± 0.12	3.39 ± 0.03
AIMD-c charge	33.16 ± 0.13	4.23 ± 0.03
AIMD-l charge	34.57 ± 0.14	3.98 ± 0.03
AIMD-b charge	30.72 ± 0.14	2.43 ± 0.03
Exp.	38.24[c]	4.27[d]

[a]Predicted value taken from ref 103. [b]Experimental value taken from ref 104. [c]Predicted value taken from ref 103. [d]Experimental value taken from ref 104.

Table 8. Computed Normal Melting Temperatures (K) for [BMIM][PF6] and [EMIM][PF6] Using the PSCP Method[a]

	[BMIM][PF6]	[EMIM][PF6]
full charge	292	382
scaled charge	245	297
AIMD-c charge	284	330
AIMD-l charge	260	332
AIMD-b charge	308	289
Exp.	284[b]	338[c]

[a]Using the procedure described previously,[96] the statistical error was estimated to be within ±1 K for each case. [b]Experimental value taken from ref 78. [c]Experimental value taken from ref 1.

Table 9. Computed Free Energy Difference (kcal/mol) at the Reference Temperature for [BMIM][PF6] and [EMIM][PF6] along the PSCP Cycle[a]

	[BMIM][PF6] (340 K)	[EMIM][PF6] (380 K)
full charge	−0.3608(17)	−0.0242(11)
scaled charge	−0.9791(15)	−0.9994(12)
AIMD-c charge	−0.5151(16)	−0.6467(11)
AIMD-l charge	−0.8322(14)	−0.6059(10)
AIMD-b charge	−0.1676(15)	−1.0994(10)

[a]The values in parentheses depict the statistical uncertainty in the final digits.

avoided. With periodic boundary conditions, the charge transfer and polarization observed for ionic liquids in their condensed phase is implicitly included. The method was applied to two ionic liquids, 1-*n*-butyl-3-methylimidazolium hexafluorophosphate ([BMIM][PF6]) and 1-ethyl-3-methylimidazolium hexafluorophosphate ([EMIM][PF6]), and a total charge of ±0.8 e was found for the cation and anion, respectively. The charges obtained this way were denoted as "AIMD-c charge".

Four more sets of atomic charges were also derived. The "full charge" was derived from DFT calculation on isolated ions in a vacuum, so no charge transfer or polarization was considered; the total charge on each ion was unity. The second set of charges was obtained by uniformly scaling the full charge by a

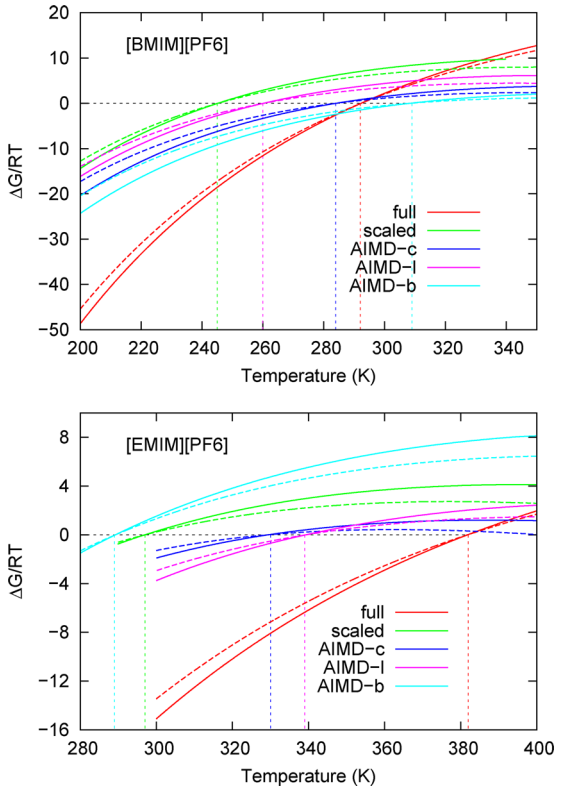

Figure 12. The free energy difference between the crystal and liquid phases as a function of temperature. The melting temperature was determined by finding the temperature where the free energy difference vanishes (indicated by dashed lines). The melting temperatures are summarized in Table 8. The AIMD-c charge results agree with experimental values very well for both ILs studied in this work.

factor of 0.8 to empirically represent the effect of charge transfer and polarization in the condensed phase. The "scaled charge" has the same charge magnitude on each ion as the AIMD-c charges, but the charge distribution among atoms is different, especially in the anion. The other two sets of atomic charges were derived from liquid phase AIMD simulations, the derivation of which are at least 40 times more expensive than the AIMD-c charge in terms of computational time.

Combined with the general Amber force field, molecular dynamics simulations were carried out for the two ionic liquids with the five sets of charges. The system properties were calculated, and the performance of the five sets of charges was discussed.

For static properties like density, liquid phase structure in terms of radial distribution function, and spatial distribution functions, the results using the scaled charge and all AIMD charges are similar to each other and the liquid densities are systematically underestimated by about 6%. The full charge liquid structures were similar to the scaled and AIMD charge results, whereas the full charge liquid densities agree slightly better with the experimental results than the results obtained with scaled or AIMD charges. However, the full charge significantly underestimated the self-diffusivities of the ions for both ILs. The dynamic properties of both ILs were well reproduced by simulations using the four sets of reduced charges, although a difference between the scaled and AIMD charges was observed. The best results were obtained from scaled charges and AIMD-c charges. Relative to static

dx.doi.org/10.1021/jp3037999 | J. Phys. Chem. B 2012, 116, 10036−10048

properties, dynamic properties are more sensitive to the charge distributions and magnitude. Thermodynamic properties such as fusion enthalpy and melting temperatures are also extremely sensitive to the charge magnitude and distribution. We find that the AIMD-c charges gave much better enthalpies of fusion and melting points than any other set of charges. Vaporization enthalpies also differed between the five charge sets, but the lack of reliable experimental data for this property makes it hard to say which set of charges performs best. Overall, the AIMD-c charges derived from crystal phase AIMD simulation were found to perform better than the other four sets of charges studied in the current work, providing a simple yet reliable approach to derive atomic charges for condensed phase simulation of ionic liquids.

Focusing on how ion charge magnitude and distribution affect molecular simulation results, the original GAFF force field was used in the current study with the five sets of charge parameters. The performance of each set of charges can be improved by adjusting other parameters in the force field, for example, by tuning the vdW parameters.[47] Even without doing so, for both ionic liquids studied in the current work, the AIMD-c charges derived from crystal phase DFT calculation were found to reproduce available experimental values very well for all properties studied in the current work. Considering the potentially huge amount of ionic liquids, this can be an essential advantage, since fitting parameters for every ionic liquid can be a tedious task.

In the current study, the PBE functional form and ESP method with default options have been applied to demonstrate the method. Obviously, other combinations of functional forms and partial charge derivation approaches can be applied to the crystal phase as well. By choosing these and other parameters in the AIMD simulation carefully, it may be possible to further improve the performance of the derived partial charges in condensed phase ionic liquid simulations. This could be the focus of future studies.

An obvious drawback of the proposed charge fitting procedure is the requirement of a crystal structure as input. With studies on ionic liquids exploding during the past years, more and more crystal structures are being reported. The proposed method will also benefit from the significant progress made during the past years in the theoretical calculation based crystal structure prediction.[105]

AUTHOR INFORMATION

Corresponding Author

*E-mail: ed@nd.edu.

Notes

The authors declare no competing financial interest.

ACKNOWLEDGMENTS

This material is based upon work supported by the Air Force Office of Scientific Research under AFOSR Award Number FA9550-10-1-0244 and by the Advanced Research Projects Agency - Energy (ARPA-E), U.S. Department of Energy, under Award Number DE-AR0000094. Computational resources were provided by the Center for Research Computing (CRC) at the University of Notre Dame.

REFERENCES

(1) Reichert, W. M.; Holbrey, J. D.; Swatloski, R. P.; Gutowski, K. E.; Visser, A. E.; Nieuwenhuyzen, M.; Seddon, K. R.; Rogers, R. D. *Crys. Growth Des.* **2007**, *7*, 1106−1114.
(2) Maginn, E. J. *Acc. Chem. Res.* **2007**, *40* (11), 1200−1207.
(3) Maginn, E. J. *J. Phys.: Condens. Matter* **2009**, *21* (37), 373101.
(4) Gurkan, B.; Goodrich, B. F.; Mindrup, E. M.; Ficke, L. E.; Massel, M.; Seo, S.; Senftle, T. P.; Wu, H.; Glaser, M. F.; Shah, J. K.; Maginn, E. J.; Brennecke, J. F.; Schneider, W. F. *J. Phys. Chem. Lett.* **2010**, *1* (24), 3494−3499.
(5) Anderson, J. L.; Dixon, J. K.; Brennecke, J. F. *Acc. Chem. Res.* **2007**, *40* (11), 1208−1216.
(6) Brennecke, J. F.; Gurkan, B. E. *J. Phys. Chem. Lett.* **2010**, *1*, 3459−3464.
(7) Yan, T.; Burnham, C.; Del Popolo, M.; Voth, G. *J. Phys. Chem. B* **2004**, *108* (32), 11877−11881.
(8) Wang, Y.; Jiang, W.; Yan, T.; Voth, G. A. *Acc. Chem. Res.* **2007**, *40* (11), 1193−1199.
(9) Yan, T.; Wang, Y.; Knox, C. *J. Phys. Chem. B* **2010**, *114*, 6886−6904.
(10) Yan, T.; Wang, Y.; Knox, C. *J. Phys. Chem. B* **2010**, *114*, 6905−6921.
(11) Schröder, C. *Phys. Chem. Chem. Phys.* **2012**, *14*, 3089.
(12) Zhang, S.; Lu, X.; Zhang, Y.; Zhou, Q.; Sun, J.; Han, L.; Yue, G.; Liu, X.; Cheng, W.; Li, S. In *Molecular thermodynamics of complex systems*; Lu, X., Hu, Y., Eds.; Structure and Bonding, Vol. *131*; Springer: Verlag Berlin Heidelberg, 2009; pp 143−191.
(13) Ma, Z.; Yu, J.; Dai, S. *Adv. Mater.* **2010**, *22* (2), 261−285.
(14) Krekeler, C.; Dommert, F.; Schmidt, J.; Zhao, Y. Y.; Holm, C.; Berger, R.; Delle Site, L. *Phys. Chem. Chem. Phys.* **2010**, *12* (8), 1817−1821.
(15) Fumino, K.; Wulf, A.; Ludwig, R. *Angew. Chem., Int. Ed.* **2008**, *47* (45), 8731−8734.
(16) Hu, X.; Liu, C.; Wu, Y.; Zhang, Z. *J. Phys. Chem. C* **2011**, *115*, 23913−23921.
(17) Hunt, P. A. *J. Phys. Chem. B* **2007**, *111*, 4844−4853.
(18) Zahn, S.; Kirchner, B. *J. Phys. Chem. A* **2008**, *112*, 8430−8435.
(19) Izgorodina, E. I.; Bernard, U. L.; Macfarlane, D. R. *J. Phys. Chem. A* **2009**, *113*, 7064−7072.
(20) Del Popolo, M. G.; Lynden-Bell, R. M.; Kohanoff, J. *J. Phys. Chem. B* **2005**, *109*, 5895−5902.
(21) Buhl, M.; Chaumont, A.; Schurhammer, R.; Wipff, G. *J. Phys. Chem. B* **2005**, *109*, 18591−18599.
(22) Bhargava, B.; Balasubramanian, S. *Chem. Phys. Lett.* **2006**, *417*, 486−491.
(23) Bagno, A.; D'Amico, F.; Saielli, G. *ChemPhysChem* **2007**, *8*, 873−881.
(24) Kirchner, B.; Seitsonen, A. P. *Inorg. Chem.* **2007**, *46*, 2751−2754.
(25) Hadi, M.; Ansari, Y. *J. Chem. Phys.* **2007**, *126*, 154502.
(26) Spickermann, C.; Thar, J.; Lehmann, S.; Zahn, S.; Hunger, J.; Buchner, R.; Hunt, P.; Welton, T.; Kirchner, B. *J. Chem. Phys.* **2008**, *129*, 104505.
(27) Thar, J.; Brehm, M.; Seitsonen, A. P.; Kirchner, B. *J. Phys. Chem. B* **2009**, *113*, 15129−15132.
(28) Zahn, S.; Thar, J.; Kirchner, B. *J. Chem. Phys.* **2010**, *132*, 124506.
(29) Mallik, B.; Siepmann, J. I. *J. Phys. Chem. B* **2010**, *114*, 12577−12584.
(30) Zahn, S.; Wendler, K.; Delle Site, L.; Kirchner, B. *Phys. Chem. Chem. Phys.* **2011**, *13*, 15083−15093.
(31) Borodin, O. *J. Phys. Chem. B* **2009**, *113*, 11463−11478.
(32) Schröder, C.; Steinhauser, O. *J. Chem. Phys.* **2010**, *133*, 154511.
(33) Zhao, W.; Leroy, F.; Heggen, B.; Zahn, S.; Kirchner, B.; Balasubramanian, S.; Muller-Plathe, F. *J. Am. Chem. Soc.* **2009**, *131*, 15825−15833.
(34) Wu, H.; Shah, J. K.; Tenney, C. M.; Rosch, T. W.; Maginn, E. J. *Ind. Eng. Chem. Res.* **2011**, *50* (15, SI), 8983−8993.
(35) Tsuzuki, S.; Matsumoto, H.; Shinoda, W.; Mikami, M. *Phys. Chem. Chem. Phys.* **2011**, *13*, 5987−5993.
(36) Pensado, A.; Gomes, M. F. C.; Canongia Lopes, J. N.; Malfreyt, P.; Padua, A. A. H. *Phys. Chem. Chem. Phys.* **2011**, *13*, 13518−13526.
(37) Babarao, R.; Dai, S.; Jiang, D.-e. *J. Phys. Chem. B* **2011**, *115*, 9789−9784.

(38) Morrow, T. I.; Maginn, E. J. *J. Phys. Chem. B* **2002**, *106*, 12807−12813.
(39) Shah, J. K.; Brennecke, J. F.; Maginn, E. J. *Green Chem.* **2002**, *4*, 112−118.
(40) de Andrade, J.; Boes, E. S.; Stassen, H. *J. Phys. Chem. B* **2002**, *106*, 13344−13351.
(41) de Andrade, J.; Boes, E. S.; Stassen, H. *J. Phys. Chem. B* **2002**, *106*, 3546−3548.
(42) Liu, Z.; Huang, S.; Wang, W. *J. Phys. Chem. B* **2004**, *108*, 12978−12989.
(43) Del Popolo, M. G.; Voth, G. A. *J. Phys. Chem. B* **2004**, *108*, 1744−1752.
(44) Urahata, S. M.; Ribeiro, M. C. *J. Chem. Phys.* **2004**, *120*, 1855−1863.
(45) Youngs, T. G.; Del Popolo, M. G.; Kohanoff, J. *J. Phys. Chem. B* **2006**, *110*, 5697−5707.
(46) Micaelo, N. M.; Baptista, A. M.; Soares, C. *J. Phys. Chem. B* **2006**, *110*, 14444−14451.
(47) Koddermann, T.; Paschek, D.; Ludwig, R. *ChemPhysChem* **2007**, *8*, 2464−2470.
(48) Dommert, F.; Wendler, K.; Berger, R.; Delle Site, L.; Holm, C. *ChemPhysChem* **2012**, *13*, 1625−1637.
(49) Jorgensen, W.; Maxwell, D. S.; Tirado-Rives, J. *J. Am. Chem. Soc.* **1996**, *118*, 11225−11236.
(50) Cornell, W. D.; Cieplak, P.; Bayly, C. I.; Gould, I. R.; Merz, K. M.; Ferguson, D. M.; Spellmeyer, D. C.; Fox, T.; Caldwell, J. W.; Kollman, P. A. *J. Am. Chem. Soc.* **1995**, *117*, 5179−5197.
(51) Scott, W. R.; Hunenberger, P. H.; Tirono, I. G.; Mark, A. E.; Billeter, S. R.; Fennen, J.; Torda, A. E.; Huber, T.; Kruger, P.; van Gunsteren, W. F. *J. Phys. Chem. A* **1999**, *103*, 3596−3607.
(52) MacKerell, A. D.; J.; Bashford, D.; Bellott, M.; Dunbrack, R. L.; Evanseck, J. D.; Field, M. J.; Fischer, S.; Gao, J.; Guo, H.; Ha, S.; et al. *J. Phys. Chem. B* **1998**, *102*, 3586−3616.
(53) Canongia Lopes, J. N.; Deschamps, J.; Padua, A. A. *J. Phys. Chem. B* **2004**, *108*, 2038−2047.
(54) Canongia Lopes, J. N.; Deschamps, J.; Padua, A. A. *J. Phys. Chem. B* **2004**, *108*, 11250.
(55) Canongia Lopes, J. N.; Padua, A. A. *J. Phys. Chem. B* **2004**, *108*, 16893−16898.
(56) Canongia Lopes, J. N.; Padua, A. A. *J. Phys. Chem. B* **2006**, *110*, 19586−19592.
(57) Canongia Lopes, J. N.; Padua, A. A.; Shimizu, K. *J. Phys. Chem. B* **2008**, *112*, 5039−5046.
(58) Liu, Z.; Wu, X.; Wang, W. *Phys. Chem. Chem. Phys.* **2006**, *8*, 1096−1104.
(59) Liu, Z.; Chen, T.; Bell, A.; Smit, B. *J. Phys. Chem. B* **2010**, *114*, 4572−4582.
(60) Liu, Z.; Chen, T.; Bell, A.; Smit, B. *J. Phys. Chem. B* **2010**, *114*, 10692.
(61) Zhong, X.; Liu, Z.; Cao, D. *J. Phys. Chem. B* **2011**, *115*, 10027−10040.
(62) Sambasivarao, S. V.; Acevedo, O. *J. Chem. Theory Comput.* **2009**, *5*, 1038−1050.
(63) Wang, Y.; Izvekov, S.; Yan, T.; Voth, G. A. *J. Phys. Chem. B* **2006**, *110*, 3564−3575.
(64) Bhargava, B.; Balasubramanian, S.; Klein, M. L. *Chem. Commun.* **2008**, 3339−3351.
(65) Chaban, V. V.; Voroshylova, I. V.; Kalugin, O. N. *Phys. Chem. Chem. Phys.* **2011**, *13*, 7910−7920.
(66) Men, S.; Lovelock, K. R.; Licence, P. *Phys. Chem. Chem. Phys.* **2011**, *13*, 15244−15255.
(67) Hurisso, B. B.; Lovelock, K. R.; Licence, P. *Phys. Chem. Chem. Phys.* **2011**, *13*, 17737−17748.
(68) Bhargava, B.; Balasubramanian, S. *J. Chem. Phys.* **2007**, *127*, 114510.
(69) Chaban, V. *Phys. Chem. Chem. Phys.* **2011**, *13*, 16055−16062.
(70) Chaban, V. V.; Prezhdo, O. V. *Phys. Chem. Chem. Phys.* **2011**, *13*, 19345−19354.
(71) Chaumont, A.; Schurhammer, R.; Wipff, G. *J. Phys. Chem. B* **2005**, *109*, 18964−18973.
(72) Youngs, T. G.; Hardacre, C. *ChemPhysChem* **2008**, *9*, 1548−1558.
(73) Yasaka, Y.; Klein, M.; Nakahara, M.; Matubayasi, N. *J. Chem. Phys.* **2011**, *134*, 191101.
(74) Liu, H.; Maginn, E. J. *J. Chem. Phys.* **2011**, *135*, 124507.
(75) Schmidt, J.; Krekeler, C.; Dommert, F.; Zhao, Y.; Berger, R.; Delle Site, L.; Holm, C. *J. Phys. Chem. B* **2010**, *114*, 6150−6155.
(76) Wendler, K.; Zahn, S.; Dommert, F.; Berger, R.; Holm, C.; Kirchner, B.; Delle Site, L. *J. Chem. Theory Comput.* **2011**, *7*, 3040−3044.
(77) Wendler, K.; Dommert, F.; Zhao, Y.; Berger, R.; Holm, C.; Delle Site, L. *Faraday Discuss.* **2012**, *154*, 111−132.
(78) Dibrov, S.; Kochi, J. K. *Acta Crystallogr.* **2006**, *C62*, o19−o21.
(79) CPMD, http://www.cpmd.org/, Copyright IBM Corp 1990−2008, Copyright MPI fur Festkorperforschung Stuttgart 1997−2001.
(80) Perdew, J. P.; Burke, K.; Ernzerhof, M. *Phys. Rev. Lett.* **1996**, *77*, 3865−3868.
(81) Perdew, J. P.; Burke, K.; Ernzerhof, M. *Phys. Rev. Lett.* **1997**, *78*, 1396.
(82) Troullier, N.; Martins, J. L. *Phys. Rev. B* **1991**, *43*, 1993−2006.
(83) Singh, U. C.; Kollman, P. A. *J. Comput. Chem.* **1984**, *5*, 129−145.
(84) Frisch, M. J.; Trucks, G. W.; Schlegel, H. B.; Scuseria, G. E.; Robb, M. A.; Cheeseman, J. R.; Scalmani, G.; Barone, V.; Mennucci, B.; Petersson, G. A.; et al.; *Gaussian 09*, revision A.1; Gaussian, Inc.: Wallingford, CT, 2009.
(85) Bayly, C.; Cieplak, P.; Cornell, W. D.; Kollman, P. A. *J. Phys. Chem.* **1993**, *97*, 10269−10280.
(86) Blöchl, P. *J. Chem. Phys.* **1995**, *103*, 7422−7428.
(87) Cp2k, http://www.cp2k.org.
(88) Goedecker, S.; Teter, M.; Hutter, J. *Phys. Rev. B* **1996**, *54*, 1703−1710.
(89) Hartwigsen, C.; Goedecker, S.; Hutter, J. *Phys. Rev. B* **1998**, *58*, 3641−3662.
(90) Wang, J.; Wolf, R. M.; Caldwell, J. W.; Kollman, P. A.; Case, D. A. *J. Comput. Chem.* **2004**, *25*, 1157−1174.
(91) Plimpton, S. *J. Comput. Phys.* **1995**, *117*, 1−19.
(92) Veld, P. J. I.; Ismail, A. E.; Greest, G. S. *J. Chem. Phys.* **2007**, *127*, 144711.
(93) Hoover, W. G. *Phys. Rev. A* **1985**, *31*, 1695−1697.
(94) Shinoda, W.; Shiga, M.; Mikami, M. *Phys. Rev. B* **2004**, *69*, 134103.
(95) Zhang, Y.; Maginn, E. J. *J. Chem. Phys.* **2012**, *136*, 144116.
(96) Jayaraman, S.; Maginn, E. J. *J. Chem. Phys.* **2007**, *127* (21), 214504.
(97) Gu, Z.; Brennecke, J. F. *J. Chem. Eng. Data* **2002**, *47*, 339−345.
(98) Taguchi, R.; Machida, H.; Sato, Y.; Smith, R. L., Jr. *J. Chem. Eng. Data* **2009**, *54*, 22−27.
(99) Umecky, T.; Kanakubo, M.; Ikushima, Y. *Fluid Phase Equilib.* **2005**, *228−229*, 329−333.
(100) Schroder, C.; Steinhauser, O. *J. Chem. Phys.* **2008**, *128*, 224503.
(101) Gutowski, K. E.; Maginn, E. J. *J. Am. Chem. Soc.* **2008**, *130*, 14690−14704.
(102) Phillips, J. *Rep. Prog. Phys.* **1996**, *59*, 1133−1207.
(103) Deyko, A.; Hessey, S. G.; Licence, P.; Chernikova, E. A.; Krasovskiy, V. G.; Kustov, L. M.; Jones, R. G. *Phys. Chem. Chem. Phys.* **2012**, *14*, 3181−3193.
(104) Domanska, U.; Marciniak, A. *J. Chem. Eng. Data* **2003**, *48*, 451−456.
(105) Day, G. M.; Cooper, T. G.; Cruz-Cabeza, A. J.; Hejczyk, K. E.; Ammon, H. L.; Boerrigter, S. X.; Tan, J. S.; Valle, R. G. D.; Venuti, E.; Jose, J.; et al. *Acta Crystallogr.* **2009**, *B65*, 107−125.
(106) Zech, O.; Stoppa, A.; Buchner, R.; Kunz, W. *J. Chem. Eng. Data* **2010**, *55*, 1774−1778.